Effect of Milling Time on Structural Evolution and Mechanical Properties of Garnet Reinforced EN AW6082 Composites

M. RAVIATHUL BASARIYA, V.C. SRIVASTAVA, and N.K. MUKHOPADHYAY

The morphology, structure, and hardness variations of garnet reinforced EN AW6082 Al-alloy composites have been investigated. High-energy ball milling of EN AW6082 Al-alloy powder, with and without garnet reinforcement, was performed under argon atmosphere for various duration, *i.e.*, up to 50 hours. The study aimed at exploring the role of alloying elements and hard reinforcement particles on the structural evolution at different stages of mechanical milling. The composite powders were characterized in terms of the morphological variation, microstructural evolution, and thermal stability. Conventional microindentation and nanoindentation measurements were carried out on the individual powders as well as composite particles to estimate the changes in the mechanical properties of the composites with milling time. The results reveal that incorporation of hard garnet particles hastens the milling effect and leads to significant improvement in hardness and modulus of unreinforced pure aluminum and aluminum alloy. This work has demonstrated the possibility of producing composites from industrial by-product, with properties better than those of aluminum alloys and aluminum-based composites.

DOI: 10.1007/s11661-014-2685-3

I. INTRODUCTION

IN the last few years, materials design and development has witnessed a considerable emphasis on strength to weight ratio, environment friendliness and cost of materials along with their better properties and performance.[1,2] Aluminum matrix composites (AMCs), which are considered to be one of such promising materials, have been widely investigated and are attracting unprecedented interest due to their possible application in high performance structural and functional components.[3–7] The properties of AMCs can be tailored by suitable combinations of the matrix alloy, type of reinforcement and processing routes to meet specific applications. This makes these composites unique in comparison to conventional unreinforced materials.[3] Development of new processing techniques such as powder metallurgy, ultrasonic assisted casting, and friction stir casting are being used for the production of AMCs. However, powder metallurgy, employing mechanical alloying during high-energy ball milling, is considered as a promising route. This technique ensures a homogenous distribution of refined hard reinforcement particles and significant grain size refinement of matrix alloy by the repeated welding and fracturing.[8] Various types of materials, ranging from typical ceramic hard reinforcements, such as SiC, Al_2O_3, B_4C, and TiB_2[9–12] to more unconventional reinforcements, such as intermetallics,[13] metallic glasses,[14] quasicrystals[15], and carbon nanotubes[16] have been successfully used as reinforcements in AMCs through mechanical alloying/mechanical milling (MM) route.

The 6xxx series of Al-Mg-Si alloys have a wide range of industrial applications due to their excellent mechanical properties, good joining ability, corrosion resistance, low density, and good workability. Therefore, these alloys are considered as suitable material for structural applications. On the other hand, garnet, an industrial by-product of the rare earth oxide extraction from beach sand, has been found to be one of the potential reinforcement options. As garnet is cheap, abundantly available and has a Moh's hardness of 6.5 to 7.0, which is nearly equal to that of SiC, it can be used as a suitable reinforcement for Al matrix composite. Khadem *et al.*[9] showed that the addition of hard SiC particles accelerates the effect of milling process, leading to faster work hardening rate and fracture of aluminum matrix. Furthermore, aluminium shows better crystallite size refinement during ball milling in the presence of SiC particles. Rodrigues *et al.*[17] have reported that SiC is superior to other reinforcements in relation to strengthening by way of higher values of Vickers hardness of the composite. In spite of the available literature on corrosion resistance and sliding wear behavior of garnet particulate-reinforced Al alloys,[18,19] the effect of garnet on the structural/morphological behavior and mechanical properties of aluminium alloys as well as nanocomposite powders is not yet fully understood. Therefore, the present investigation aims at studying the effect of milling time, role of alloying elements and dispersion of

M. RAVIATHUL BASARIYA, Doctoral Student, is with the CSIR-National Metallurgical Laboratory, Jamshedpur 831007, India, and also with the Department of Metallurgical Engineering, Indian Institute of Technology (BHU), Varanasi 221005, India. V.C. SRIVASTAVA, Principal Scientist, is with the CSIR-National Metallurgical Laboratory. Contact e-mails: vcsrivas@gmail.com; vcsrivas@nmlindia.org N.K. MUKHOPADHYAY, Professor, is with the Department of Metallurgical Engineering, Indian Institute of Technology (BHU).

Manuscript submitted August 19, 2014.
Article published online December 3, 2014

garnet particulates on the structure, morphology, and mechanical properties of commercial aluminium and EN AW6082 Al-Si-Mg alloy composite powders produced by high-energy ball milling.

II. EXPERIMENTAL PROCEDURE

A. *Materials*

Inert gas atomized powders of aluminum alloy, grade EN AW6082 with 99 pct purity, having particle size <75 μm (supplied by Kemphasol Ltd., India) and aluminum powder of 99.7 pct purity (Merck, Germany) were used as a matrix material. Beach sand garnet powder of 99.5 pct purity with a particulate size range of 50 to 100 μm (supplied by Indian Rare Earths Limited, Manavalakurichi, India) was used as the reinforcement. The chemical composition of EN AW6082 Al-alloy powder and average chemical composition of reinforcement garnet particles are given in Tables I and II.

B. *Ball Milling*

High-energy ball milling of matrix powders and reinforcement (5 wt pct) was carried out in a high energy eccentric ball mill (Fritsch P-6 Pulverisette). The vials and balls were made of hardened stainless steel. To prevent the powders from oxidation during processing, the ball milling vials were evacuated and then filled with 99.9 pct pure argon gas. The milling operation was performed under toluene, a process control agent, to prevent the formation of oxides during milling and to minimize the extreme tendency of aluminum to get welded during milling. The alloy powders were milled up to a maximum duration of 50 hours with a ball to powder weight ratio of 10:1 at 300 rpm. To avoid over-heating during milling, experiments were paused for 5 minutes periodically after every 20 minutes of milling. The milling operation was intermittently stopped after milling times of 10, 20, 30, 40, and 50 hours for drawing samples. The milled powder samples were characterized to find out the sequence of structural evolution and the extent of alloying.

C. *Materials Characterization*

The identity and sequence of phase evolution at different stages of MM were evaluated by X-ray diffraction (XRD) analysis, which was carried out using an automated D8 Discover Bruker diffractometer with Cu K_α (λ = 0.15406 nm) radiation operated at 40 kV/30 mA and at a scanning speed of 2 deg/min. The average crystallite size and lattice micro-strain of the milled powders were determined from the full-width at half maximum (FWHM) of diffraction peaks, using Williamson and Hall method[20] after removing the instrumental broadening.

Particle size distribution (PSD) of the powders was determined using a laser diffraction particle size analyzer (Master sizer, Malvern, U.K). The external morphology of as-received powders and milled powders was examined in scanning electron microscope. Samples were prepared by sprinkling the loose powder on an adhesive stub and then examined using secondary electron imaging mode on scanning electron microscope (SEM JEOL, 840A, Japan) equipped with energy dispersive X-ray spectroscopy (EDS). The thermal stability of milled powders was examined to study the phase decomposition/dissolution reactions, if any, using differential thermal analyzer (INS SDT-Q600) under argon atmosphere, with a heating rate of 20 °C/min. Microstructural analysis was carried out by means of FEI Tecnai-20 G^2 transmission electron microscope operated at 200 kV. For TEM sample preparation, the powder was dispersed ultrasonically in acetone and a liquid drop with dispersed particles was dried on a carbon coated Cu gird.

Microhardness measurements of the individual powder particles were carried out using standard Vickers microhardness tester (UHL-VMHT, LEICA) at a load of 10 g and dwell time of 10 seconds. The reported hardness values are an average of at least five measurements. In addition, the modulus of elasticity and hardness of the milled powders were evaluated using a MTS Nano Indentor XP employing the Oliver and Phar technique.[21] The specimens for hardness measurements were prepared by mixing a small quantity of milled powder with the mounting material Epoxicure (supplied by Buehler). The cured mounts were then polished using

Table I. Chemical Composition of the Matrix—Gas Atomized Aluminum Alloy Powder EN AW6082

Element's Concentration (wt pct)							
Si	Mg	Mn	Fe	Cr	Cu	Zn	Al
1.2	0.78	0.50	0.33	0.14	0.08	0.05	bal.

Table II. Chemical Composition of the Reinforcement Particle—Garnet

Constituent (Oxides) (wt pct)						
SiO_2	Al_2O_3	TiO_2	Fe_2O_3	CaO	MgO	MnO
36.15	19.09	0.57	32.87	3.41	7.22	0.69

standard metallographic technique. The final polishing was accomplished by 0.05 μm alumina powder suspension. The mounting material used was hard enough to support the particles under the applied load. The indentation sites on these samples were chosen to be within the grain interior and away from grain boundaries and microscopic pores.

III. RESULTS AND DISCUSSION

A. *X-ray Diffraction Analysis*

The typical XRD patterns of EN AW6082, EN AW6082/Garnet, and Al/Garnet powder mixtures at different stages of MM are shown in Figure 1. These patterns exhibit distinct major peaks corresponding to face centered cubic α-Al and weak diffraction peaks of garnet. For unreinforced EN AW6082, peaks related to alloying elements disappeared completely after 10 hours of milling, as shown in Figure 1(a). The absence of Si and Mg containing intermetallic peaks may be attributed to the gradual dissolution of these minor alloying elements into the α-Al matrix with increasing milling time. Similar results were observed by other researchers as well.[22,23] During continuous milling, α-Al peaks decreased in intensity and simultaneously peak width increased with the increase of milling time, denoting a microstructural refinement. During high-energy ball milling, the powders experience repeated collision, fracture, and cold welding. The severe plastic deformation induced by the above processes lead to grain refinement, accumulation of internal stresses that changes the lattice parameter and formation of cell structure.[24–26] Along with the cold welding event during high-energy ball milling, some powders also coat the grinding medium and/or the inner walls of the container. A thin layer of the coating is thus beneficial in preventing wear and tear of the grinding medium and also in preventing contamination of the milled powder with the debris. However, the level of contamination is very low, so the Fe peaks was not observed and can be attributed to the limitation of the filtered X-ray to detect phases with amount less than 2.0 wt pct.

Also, the XRD pattern of the milled powders evidenced that no intermetallic peak was formed and the material obtained did consist of only Al phase without any secondary phase even after 50 hours of milling. The sharp crystalline peaks (Figures 1(b) and (c)) broadened progressively with increasing milling time and refinement of grain size down to nanometer range, in both aluminum and EN AW6082, was observed. The reduction in crystallite size was due to the creation of a large numbers of linear defects, particularly dislocations, which resulted in formation of sub-cells.[27]

Figures 2(a) and (b) show the position (*i.e.*, 2θ diffraction angles) of the first intense peak Al (111) from all the milling durations. In unreinforced EN AW6082, the peak positions shift towards lower values of diffraction angle and then to higher values as the milling time increases. The displacement of Al (111)

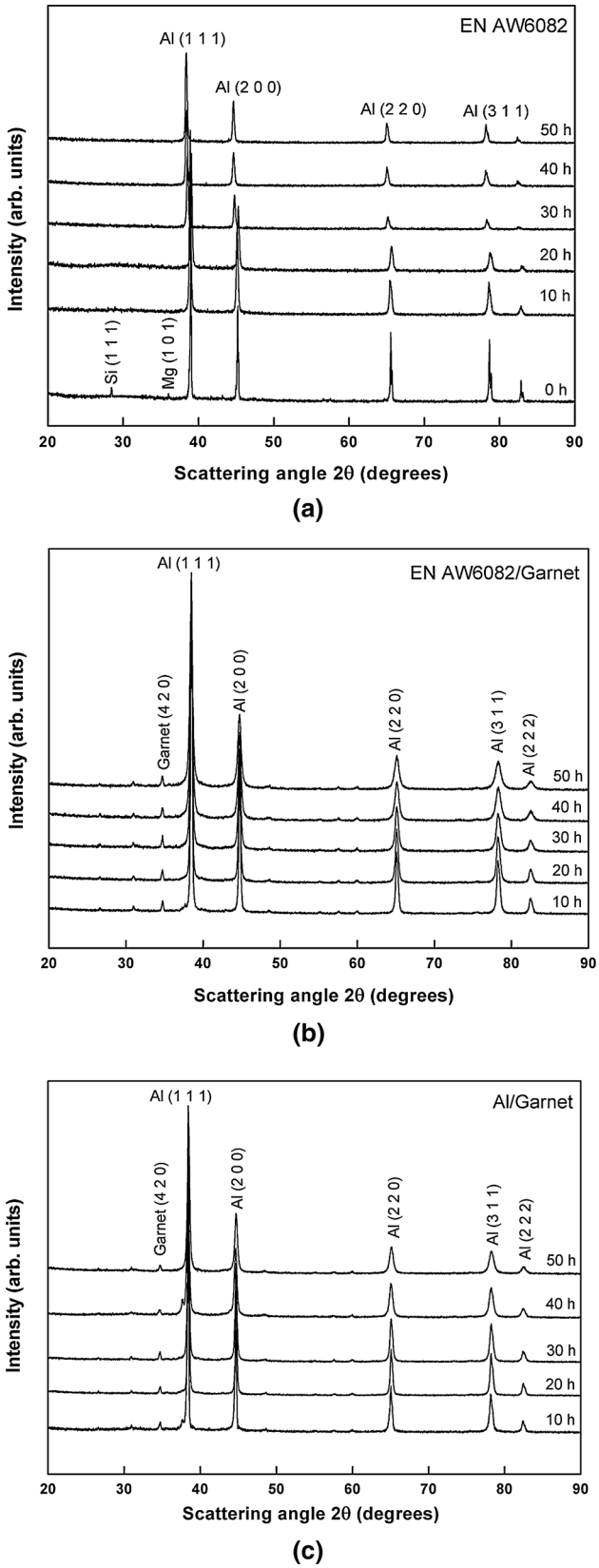

Fig. 1—XRD patterns of (*a*) unreinforced EN AW6082, (*b*) EN AW6082/Garnet, and (*c*) Al/Garnet composite powder after 10, 20, 30, 40, and 50 h of high-energy ball milling.

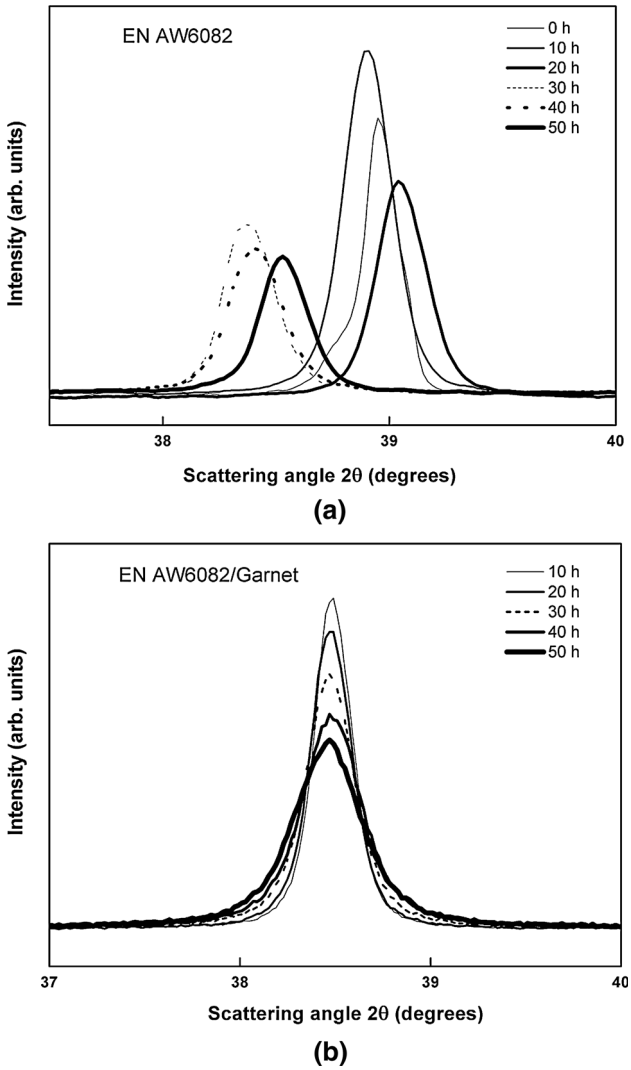

Fig. 2—Evolution of d_{111} peak intensity on powder XRD showing the broadening and reduction in intensity milled at different hours for (*a*) unreinforced EN AW6082, (*b*) ENAW6082/Garnet.

peak towards lower angles, which in turn indicates increase in Al lattice parameter, with increasing milling time suggests the gradual dissolution of alloying elements, namely, Si and Mg in the Al lattice and consequently the formation of an Al-based supersaturated solid solution after 30 hours of milling. Earlier investigations[13,23] reported similar trend and attributed the variation in lattice parameter to the solute dissolution. The peak shift towards higher angles also indicates the existence of strain in the mechanically milled matrix.[28] In composite powders, during initial stages of milling, Al peaks shift towards lower angles due to the alloying elements which start to dissolve in Al matrix and at later stages of milling no peak shifting was observed except for reduction in crystallite size due to interface structure, which has a large volume fraction in nanosize materials.[29] The dissolution of alloying elements which causes peak displacement is also hindered by the hard rigid dispersoids and hence, in general, with garnet as reinforcement the peak shift is minimal.

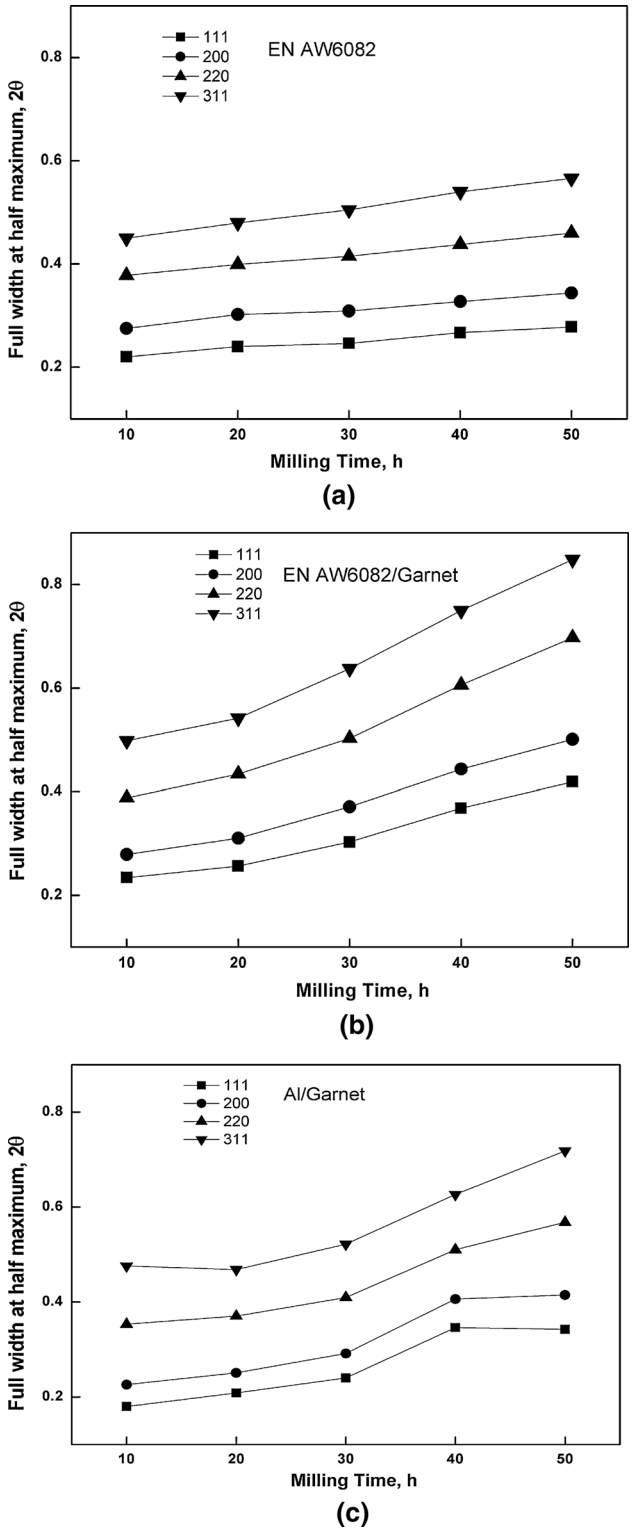

Fig. 3—Full width at half maximum intensity of diffraction planes as a function of milling time for (*a*) unreinforced EN AW6082, (*b*) EN AW6082/Garnet, and (*c*) Al/Garnet.

X-ray line broadening, in terms of FWHM, with milling for unreinforced alloy and composites is shown in Figures 3(a) through (c). It appears that the high-energy milling increased the FWHM with increasing milling time and this may be ascribed to a severe lattice

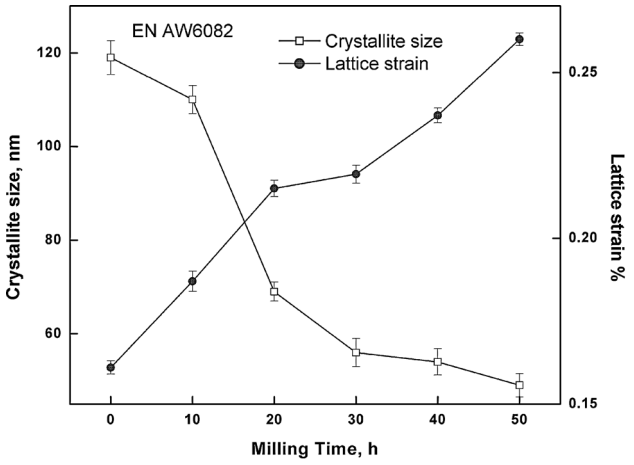

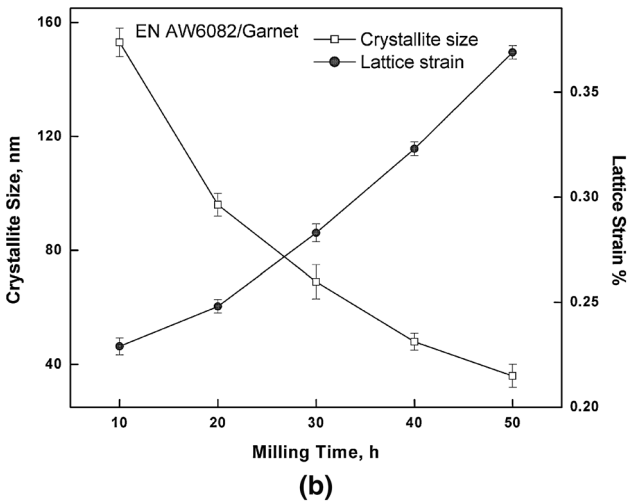

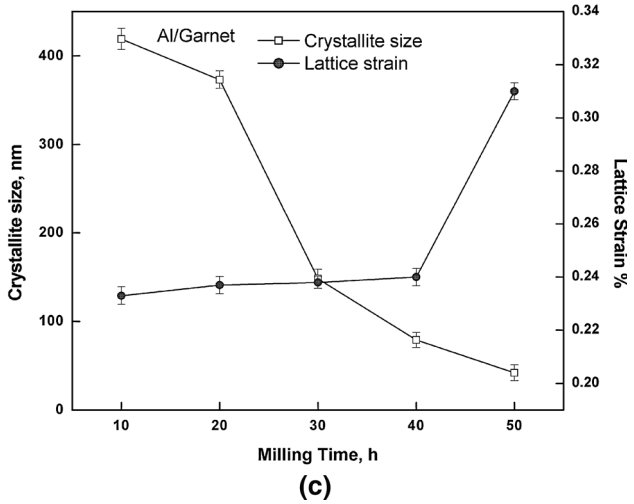

Fig. 4—Variation in crystallite size and strain rate as a function of milling time (*a*) unreinforced EN AW6082, (*b*) EN AW6082/Garnet, and (*c*) Al/Garnet.

distortion and crystallite size refinement.[30] During higher milling time the sample volume exhibiting small grains extends throughout the entire specimen, hence decreasing the effective crystallite size.[31]

Figures 4(a) through (c) show the variation of crystallite size and lattice strain with milling time for both the unreinforced as well as reinforced materials. It is clearly observed that the grain refinement in both Al/Garnet and EN AW6082/Garnet composites continued with increasing milling time due to presence of hard garnet particles and lattice distortion; and the large amount of lattice strain at final stages of milling is also due to the milling of hard reinforcement with the matrix materials. The crystallite size and microstrain of the powders milled for 50 hours was determined using Williamson–Hall plots and are given in Table III. The mean crystallite size calculated using Williamson–Hall plot was around 49, 36, and 42 nm for unreinforced EN AW6082, EN AW6082/Garnet, and Al/Garnet, respectively, for a maximum milling time of 50 hours. The rate of refinement of the internal structure (crystallite size, lattice distortion, *etc.*) varies nearly logarithmically with milling time. Furthermore, addition of garnet particles makes the grain size still finer compared to unreinforced alloy. The milled EN AW6082 and hard reinforcement have resulted in greater microstructural refinement of about 36 nm compared to pure Al matrix with garnet. In the early stages of milling, a rapid decrease in crystallite size is observed due to the fact that the balls impart high impact force and transfers high kinetic energy to the particles which experience work hardening due to generation of a high dislocation density. However, the contribution of impact force to the grain refinement decreases with milling time due the fact that the increasing dislocation density lead to lower rate of plastic deformation as the milling progresses. The reduction in rate of plastic deformation reduces the rate of dislocation generation and therefore gives rise to only small reduction in crystallite size and small increase in strain. These features were intensified in the composite powders because of the presence of hard garnet particles. In early stages of milling, severe plastic deformation of particles causes a deformed lattice with high density of dislocations. However, long milling time gives rise to nanocrystalline structure.[29] The reduction in the Al grain size, in garnet reinforced particles, can be partially ascribed to the hindrance of the dislocation movement by Orowan strengthening mechanism. This results in increased dislocation density and thus accelerated grain refinement process. Lattice parameter of the composite mixture increases in comparison to unreinforced alloy due to addition of garnet particulates and grain refinement. With decreasing grain size, the volume fraction of grain boundaries increases and this results in pressure on the interfaces and tensile stress on the lattice and consequently leads to an increase in lattice parameter.[31,32]

B. *Particle Size Distribution*

The PSD of the nano-composite powders milled for 50 hours is illustrated in Figures 5(a) through (c). Table IV presents D_{50} and D_{90} to D_{10} values related to the particle size of the composite samples. The D_{50} value represents the average particle diameter equivalent to 50 pct of the particles undersize this value. The (D_{90} to D_{10}) is indicative of the spread of PSD. It is noticeable that all the milled powders exhibit relatively a log-normal size distribution. For unreinforced EN AW6082

Table III. Mean Crystallite Size and Apparent Lattice Distortion for Powders After 10, 20, 30, 40, and 50 h of Milling

	Mean Crystallite Size (nm)					Apparent Lattice Distortion (pct)				
	Milling Time (h)									
Material	10	20	30	40	50	10	20	30	40	50
EN AW6082	110	69	56	54	49	0.187	0.215	0.219	0.237	0.260
EN AW6082/Garnet	153	96	68	48	36	0.229	0.248	0.283	0.323	0.369
Al/Garnet	419	373	148	79	42	0.233	0.237	0.238	0.244	0.312

Table IV. Variation of Characteristic Diameters of Powders After 50 h of Milling

	Characteristic Diameters (μm)	
Sample	D_{50}	$D_{90\text{-}10}$
EN AW6082	30.93	80.57
EN AW6082/Garnet	32.35	93.36
Al/Garnet	22.28	35.12

(Figure 5(a)), the PSD after 50 hours of milling shows an asymmetric behavior, which is indicative of the welding of matrix particles, and shows average particle size of 31 μm. During milling, fracture gives smaller range of particles and welding leads to larger range of particles and hence skewed distribution of the particles is obtained.[27] During MM process, cold welding and fracturing are the two main deformation mechanisms for ductile phase (Al and EN AW6082) and only fracture is possible for hard brittle garnet particles. The PSD of a material after grinding depends on the equilibrium between fracture and cold welding mechanisms.[26] Since hard materials are difficult to be abraded on their surfaces, the impact mechanism plays a dominant role and the brittle particles possess a greater tendency toward fracture rather than cold welding.[33,34] Thus, the distribution curve of composite powders shows a symmetry and broader PSD, indicating the occurrence of equilibrium between fracture and welding—a typical steady state process, a characteristic of the final stage of MM. Accordingly, the average particle diameter of the EN AW6082/Garnet composite powders was lower than that of unreinforced EN AW6082 powders.

C. *Particle Morphology and Structure*

The micrograph of as-received powder of EN AW6082 alloy shows almost a spherical morphology compared to pure Al, which revealed slightly elongated particle shape, as shown in Figures 6(a) and (b). However, the EN AW6082 does show larger initial particle size. From Figure 6(c) it is evident that the reinforcement particles are in the size range of 50 to 100 μm and have sharp edges and a faceted morphology. During ball milling, the blend of powder particles was first crushed under the impact of balls followed by cold welding process. Hence, the particle morphology changes from initial equiaxed to flattened shape due to initial pre-dominance of deformation. The final stage is characterized by the steady state process, in which the microstructural refinement occur and the morphology becomes once more equiaxed. The SEM of powders milled for 50 hours (Figures 7(a), (b), and (e)), for all the powder mixtures, showed nearly equiaxed and finer particles indicating that the milling process has reached its steady state. Figure 7(b) shows the SEM micrographs of powders milled for 50 hours and confirms the formation of layered microstructure and homogenous distribution of garnet particles in the soft aluminum matrix. Figure 7(c) shows the high magnification SEM of EN AW6082/Garnet powder morphology after 50 hours, which reveals the reinforcement particles embedded on the surface of Al matrix as indicated by arrows. It also confirms the good interfacial integrity between aluminum matrix and garnet reinforcement. The corresponding EDS spectrum (Figure 7(d)) reveals, based on the particle composition, the presence of nano-sized reinforcement particles in the Al matrix. Also, the Figure 7(f) shows the magnified view of Al/Garnet composite particle revealing the entrapment of reinforcement particles into the soft matrix as indicated by arrows. From the present study of the morphology of particles, it is evident that the matrix powder has been severely deformed, with the garnet particles well dispersed into the matrix. The composite powders milled for 50 hours indicates the formation of clusters of fine particles and heavily deformed structure less than 50 nm in size. These findings are in good agreement with the crystallite size measurements made by XRD analysis.

Figures 8(a) and (b) show the TEM micrographs of 50 hours milled EN AW6082 alloy powder. It reveals that the particles consist of equiaxed nanostructured grains with an average grain size of about 50 nm. The grain size measured from TEM micrographs is comparable with the crystallite size calculated from the XRD analysis, which yielded a value of 49 nm. The TEM micrographs of EN AW6082/Garnet and Al/Garnet composites are shown in Figures 9 and 10, respectively. These micrographs confirm the nanocrystalline structure of the composite powders based on the extensive splitting of the diffraction spots, as shown in the inset. The bright-field images (Figures 9(a) and 10(a)) show that the two phases, namely garnet particles and aluminum matrix, are completely intermixed with each other. The dark-field images (Figures 9(b) and 10(b)) clearly show deformed microstructure of grains of size less than 50 nm for both the composites. The selected area diffraction (SAD) patterns from the areas displayed

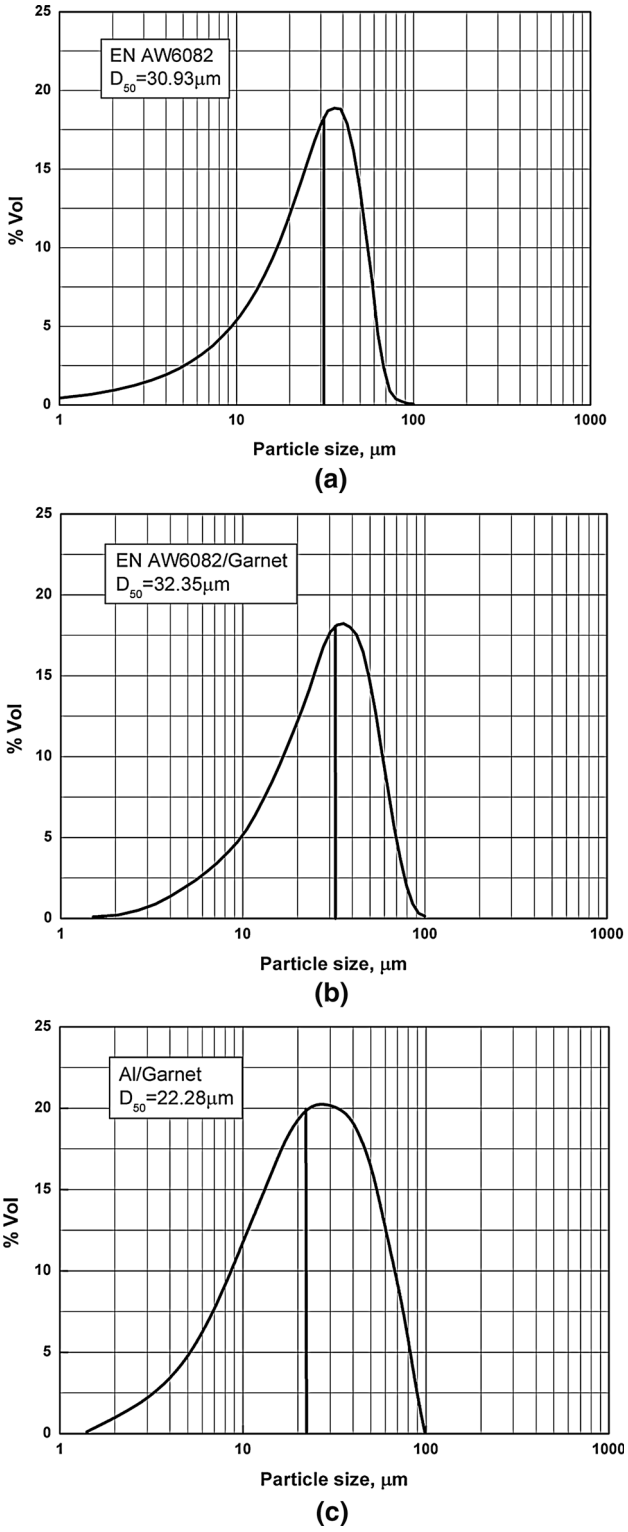

Fig. 5—Particle size distribution of milled powders after 50 h (*a*) unreinforced EN AW6082, (*b*) EN AW6082/Garnet, and (*c*) Al/Garnet.

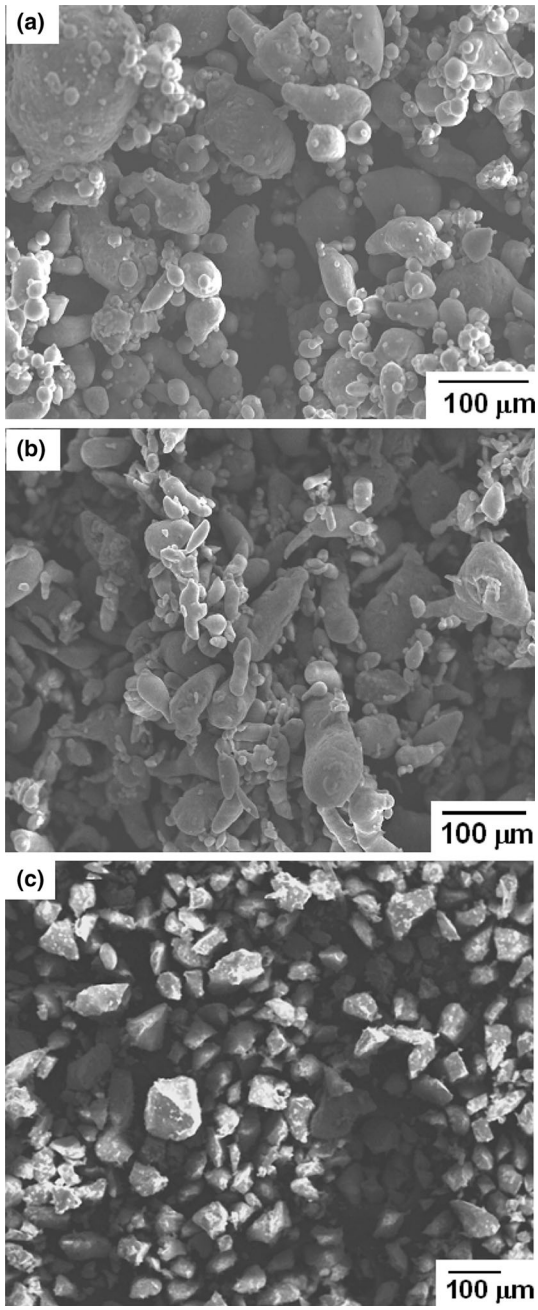

Fig. 6—SEM micrographs of as-received powders (*a*) EN AW6082, (*b*) pure Al, and (*c*) Garnet.

in the bright-field TEM images are shown as insets in Figures 9(a) and 10(a) and the planes observed were assigned as (111), (200), (220), (311), and (222) of the Al matrix-FCC phase. The complex dislocation structures, a characteristic feature of a heavily deformed material, are evident in many areas. The contrast corresponds to microstructural defects such as shear bands that occur due to the high deformation rates during milling.[35] These shear bands contain a high density of dislocations and precede the formation of substructure in the crystals and are more likely to contribute to increased hardness and reduced crystallite size.

D. *Thermal Analysis and Structural Stability*

The differential thermal analysis (DTA) plots for all the 50 hours milled nanocrystalline powder samples are

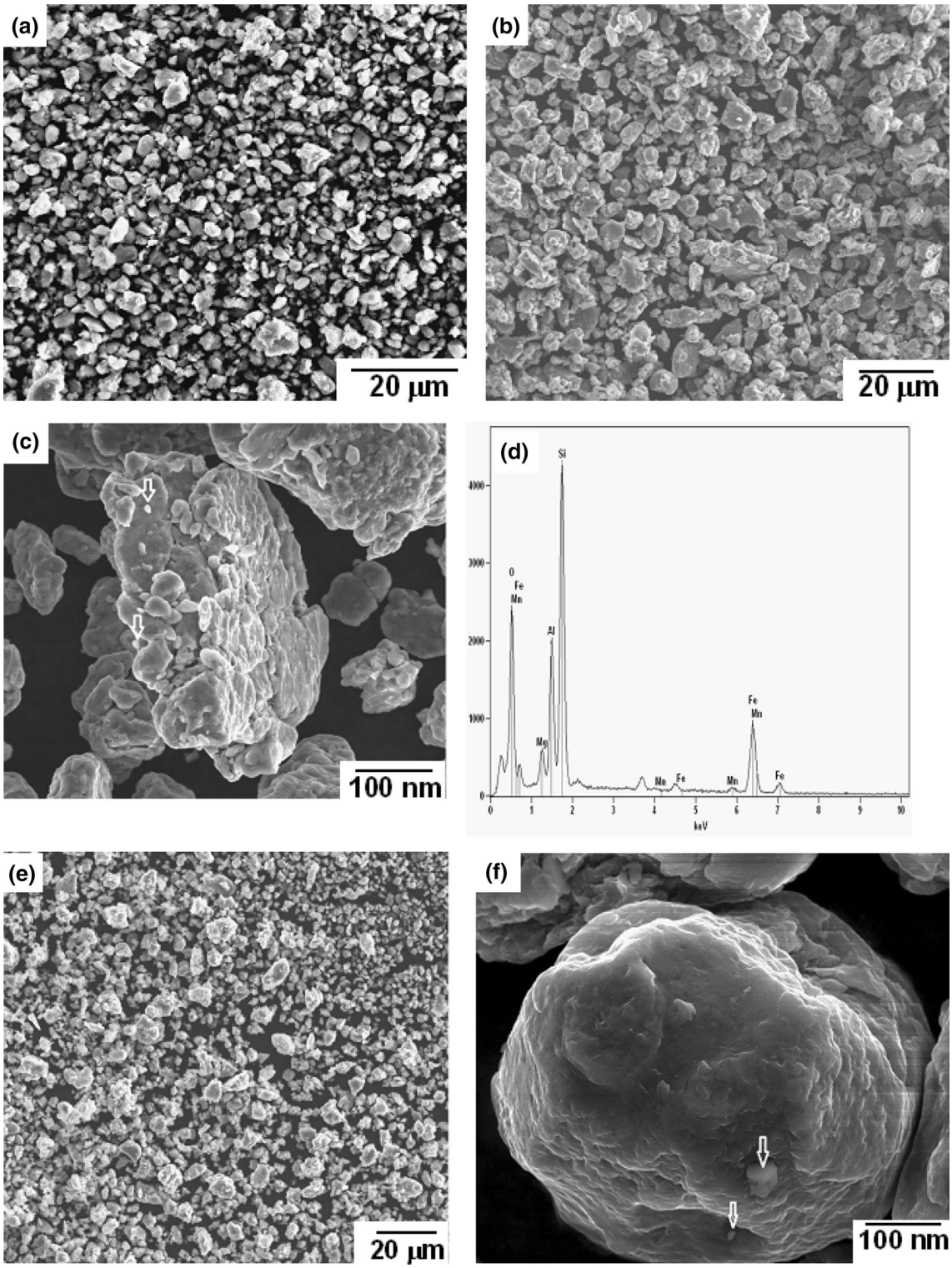

Fig. 7—Morphology of milled powders for 50 h (*a*) unreinforced EN AW6082, (*b*) EN AW6082/Garnet, (*c*) magnified view of EN AW6082/Garnet and (*d*) its corresponding EDS, (*e*) pure Al/Garnet and (*f*) magnified view of pure Al/Garnet.

shown in Figure 11. The DTA traces of all the milled powders show a sharp endothermic peak attributed to the melting of the matrix. The initial broad exothermic peak can be due to the evaporation of moisture present in the powders or some other extraneous effects. The second exothermic peak observed in the temperature range of 473 K to 773 K (200 °C to 500 °C) in the case of EN AW6082, as depicted in Figure 11, was due to the dissolution of all the precipitates into the aluminum matrix, which formed a diffusion couple with an

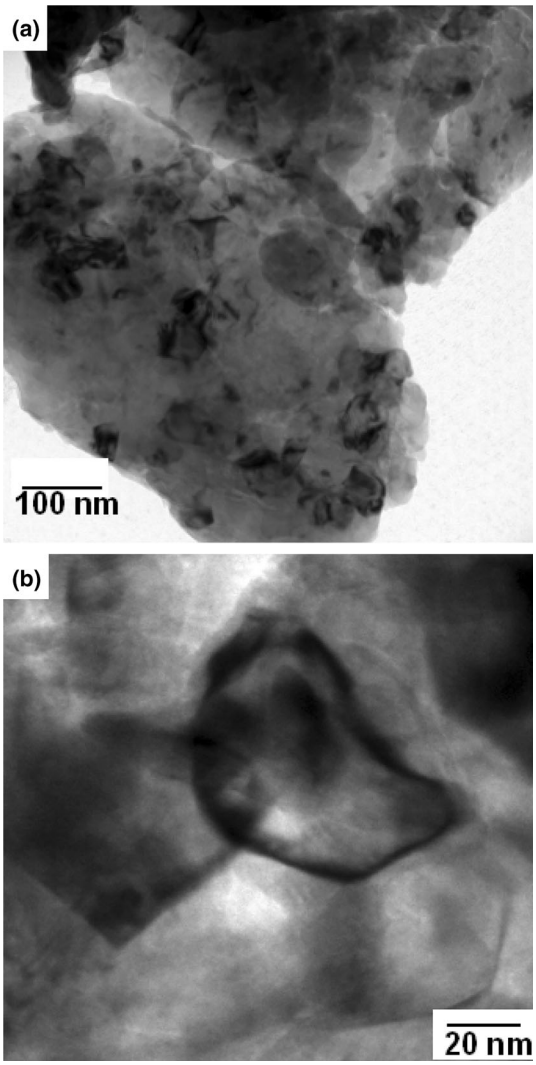

Fig. 8—(*a*) TEM micrographs of 50 h mechanically milled powder particles of EN AW8082 alloy. (*b*) Magnified view of 'a'.

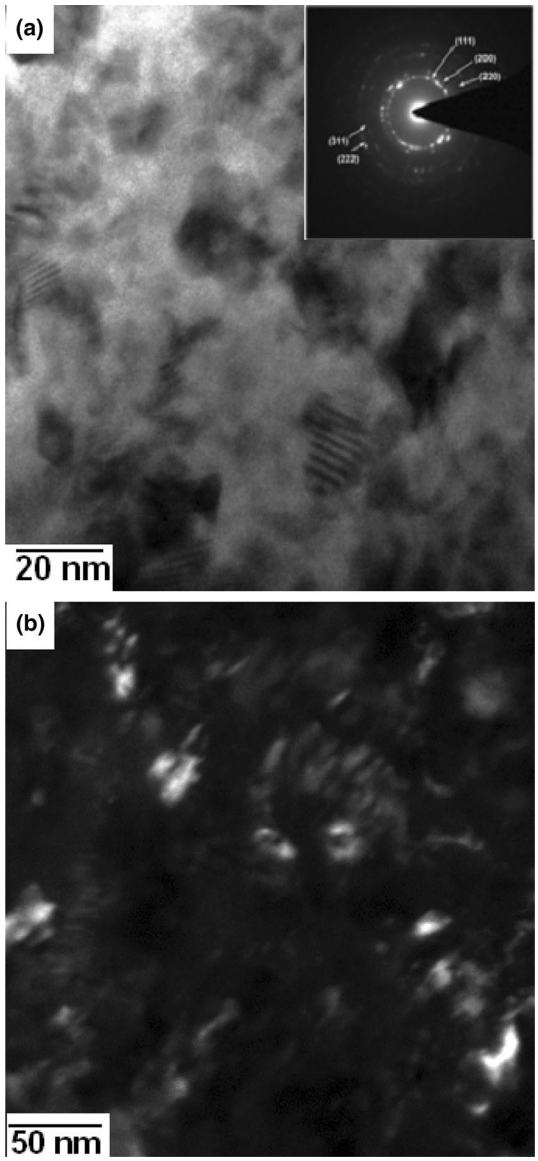

Fig. 9—(*a*) TEM bright-field image of EN AW6082/Garnet MM for 50 h and its corresponding SAD pattern and (*b*) dark-field image.

increased ball milling time.[36] The melting temperature obtained using thermal analysis was around 924 K, 925 K, and 928 K (651 °C, 652 °C, and 655 °C) for unreinforced EN AW6082, EN AW6082/Garnet, and Al/Garnet, respectively. This slight decrease in the melting point of unreinforced EN AW6082 is attributed to mechanical alloying of the powder particles which increases the surface area of the particles and surface energy of the nanocrystalline powders, when compared to other milled powders. It is also known from phase diagrams theory that when a solid solution is formed, it has a lower melting point compared with the starting pure elements.[37] The addition of reinforcement particles in the aluminum matrix has significantly altered the nature of DTA traces observed in comparison to unreinforced EN AW6082 alloy powder. The broad exothermic peak from 373 K to 804 K (100 °C to 531 °C) in EN AW6082/Garnet, and 373 K to 811 K (100 °C to 538 °C) in Al/Garnet powder mixture occurred over a period of time may be attributed to strain release and grain growth.[38,39]

E. *Hardness Variation*

The microhardness variation with milling time for unreinforced alloy and composite powder is shown in Figure 12. It is evident from the plot that both unreinforced alloy and composite powder show increasing hardness with milling time. The hardness of the Al/garnet did not increase much up to 20 hours of milling. The slower rate of increase in microhardness may be attributed to the dynamic recovery caused by high work hardening effects of deformed matrix and static recovery of highly deformed matrix with local increase of temperature in particles during collisions.[40] However, the hardness of both the composites reached closer to each other after 50 hours of milling *viz*. 313 HV for EN AW6082/Garnet and 301 HV for Al/Garnet. These values are higher in comparison with initial hardness

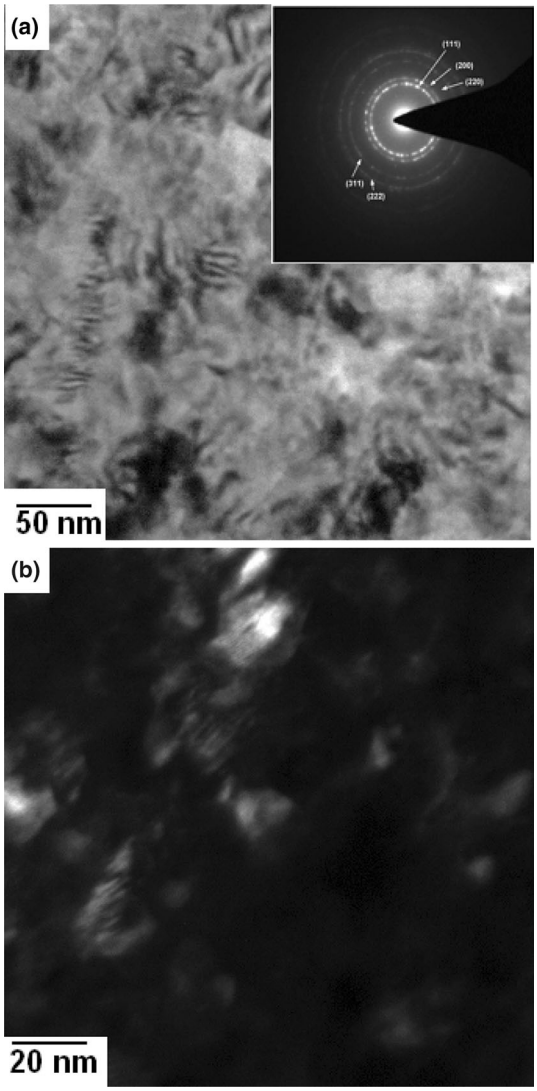

Fig. 10—(*a*) TEM bright-field image of Al/Garnet MM for 50 h and its corresponding SAD pattern and (*b*) dark-field image.

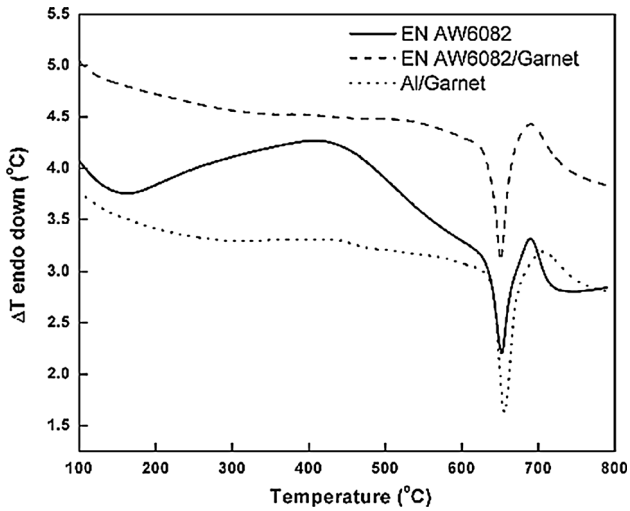

Fig. 11—DTA curves of milled powders for 50 h of unreinforced EN AW6082, EN AW6082/Garnet and Al/Garnet.

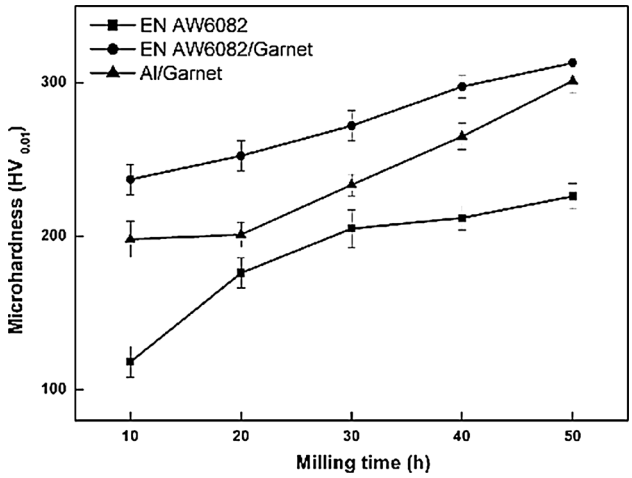

Fig. 12—Powder hardness as a function of milling time for different systems.

data of pure aluminum and aluminum alloy whose values are about 71 HV and 75 HV, respectively.

The hardening of the milled powder has been shown to be influenced by the combination of several factors: (1) lattice strain, which increases as a result of deformation during ball milling and introduces a large density of dislocation. The dislocation density contributes to the strength of the material and can be calculated on the basis of the Taylor equation,[41] (2) dispersion hardening, which can be estimated using the Orowan strengthening mechanism,[42] and (3) grain size, which is the most important factor and can be explained by the Hall–Petch relationship. The highest microhardness values are attained for EN AW6082/Garnet composite powders. The significant increase in hardness with garnet reinforcement particles can be attributed primarily to: (a) the presence of relatively harder particulates in the matrix, (b) a higher constraint to the localized matrix deformation during indentation due to their presence, (c) reduced grain size, and (d) no possibility of cluster formation.[33] To verify the relationship between microhardness and grain size, a combination of classical Hall–Petch equation[43,44] and Tabors empirical relationship,[45] $H = 3\sigma$ is used. It is known that the strength varies according to the following semi-empirical Hall–Petch equation:

$$H = H_0 + Kd^{-1/2}, \qquad [1]$$

where H_0 and K are the constants associated with the hardness measurements and d the average grain size. Figures 13(a) through (c) show the H–P plot of microhardness ($HV_{0.01}$) *vs* inverse root of grain size for milled unreinforced EN AW6082, reinforced EN AW6082 and reinforced Al composite powders, respectively. A linear fit to the experimental results of the hardness values (VHN) against the inverse of the square root of the grain size ($d^{-1/2}$) revealed the value of H_0, K, and correlation coefficient as presented in Table V. These values are higher than mechanically milled nanocrystalline pure aluminum powders reported by Hamid Abdoli *et al.*[46] which revealed value of 7.3 ± 2 MPa and 373 ± 75

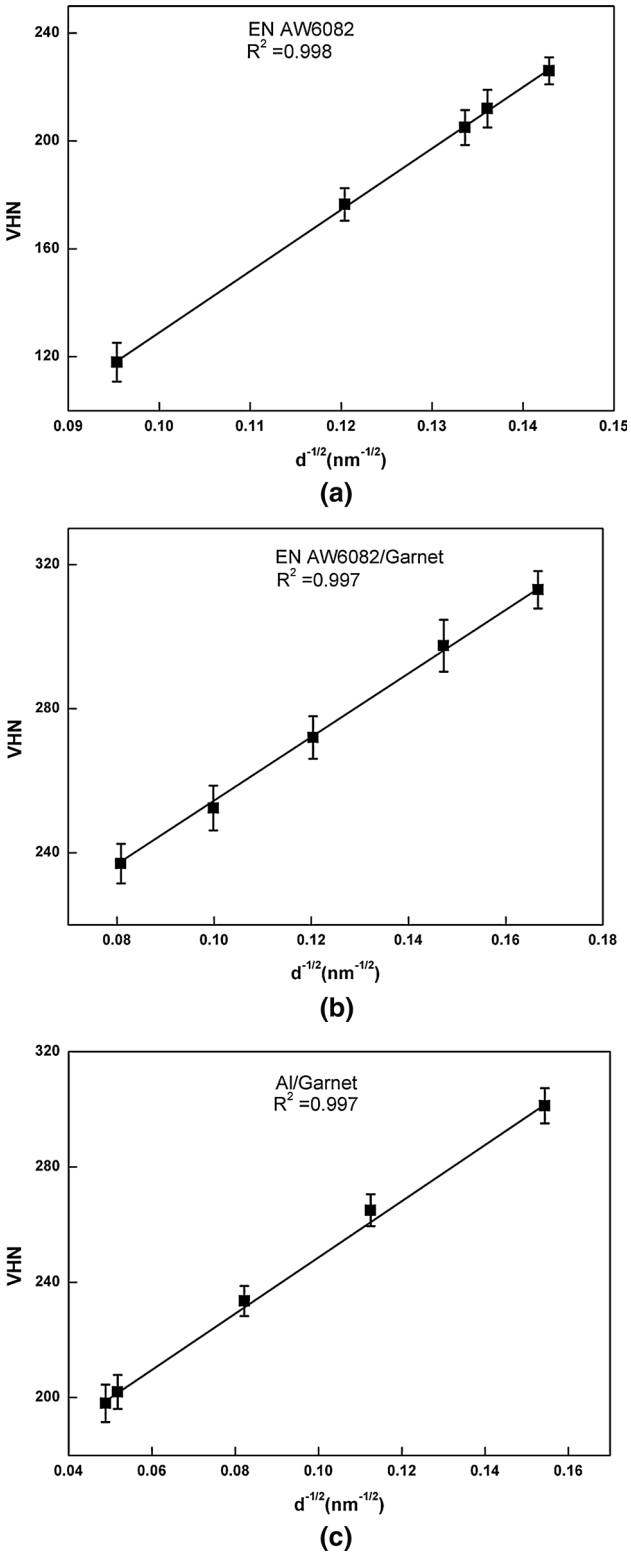

Fig. 13—Hardness of milled powders as a function of grain size (*a*) unreinforced EN AW6082, (*b*) EN AW6082/Garnet, and (*c*) Al/Garnet.

(nm)$^{1/2}$ MPa for H_0 and K, respectively, confirming that the influence of reinforcement type, size and alloying element has greater impact on the mechanical properties

Table V. Fitting Constants Obtained from Hall–Petch Equation

System	H_0 (MPa)	K (nm)$^{1/2}$	R^2
EN AW6082	32.5 ± 14	756.43 ± 140	0.998
EN AW6082/Garnet	54.6 ± 10	298.72 ± 80	0.997
Al/Garnet	50.3 ± 6.7	328.25 ± 68	0.997

of the composite powders. The slope of the linear fit in all the systems is positive and hence it can be evidenced that the above relationship holds good for the present investigation; and further the higher slope can be attributed to high density of dislocations generated during high-energy milling.[47]

The strengthening effect in particulate-reinforced metal matrix composites is attributed to three main factors involving: (i) Orowan strengthening effect, (ii) enhanced dislocation density due to the residual plastic strain caused by the difference in the coefficients of thermal expansion between the matrix and particles, and (iii) load-bearing effect of the hard reinforcements.[48]

Zhang and Chen[49] have proposed an analytical expression to predict the yield strength by incorporating the three effects mentioned above by the following equation:

$$\sigma_{yc} = \sigma_{ym}(1 + f_l)(1 + f_d)(1 + f_{Orowan}), \quad [2]$$

$$f_l = 0.5V_p, \quad [2a]$$

$$f_d = \frac{1.25G_m b}{\sigma_{ym}} \sqrt{\frac{12(T_{proc} - T_{test})(\alpha_m - \alpha_p)V_p}{bd_p(1 - V_p)}}, \quad [2b]$$

$$f_{Orowan} = \frac{0.13G_m b}{\sigma_{ym} d_p \left[\left(\frac{1}{2V_p}\right)^{1/3} - 1\right]} \ln\frac{d_p}{2b}, \quad [2c]$$

where σ_{yc} is the yield strength of MMCs, σ_{ym} is the yield strength of the monolithic matrix under the same processing conditions as those of MMCs, f_l is the improvement factor due to the load-bearing effect, f_d is the improvement factor associated with the enhanced dislocation density in the matrix induced by the thermal mismatch between the matrix and the reinforcement particles, f_{Orowan} is the improvement factor due to the Orowan strengthening effect, G_m is the shear modulus of the matrix, b is the Burgers vector of dislocations in the matrix, T_{proc} is the processing temperature, T_{test} is the test temperature, α_m is the coefficient of thermal expansion of the matrix, α_p is the coefficient of thermal expansion of the reinforcement phase, V_p is the volume fraction of reinforcement particles, and d_p is the particle size.

The model proposed by Zhang and Chen[49] was used to understand the strengthening effect of the ball-milled composite in the present study. In addition, similar strengthening model proposed by Ramakrishnan,[50] which does not take into account the Orowan strength-

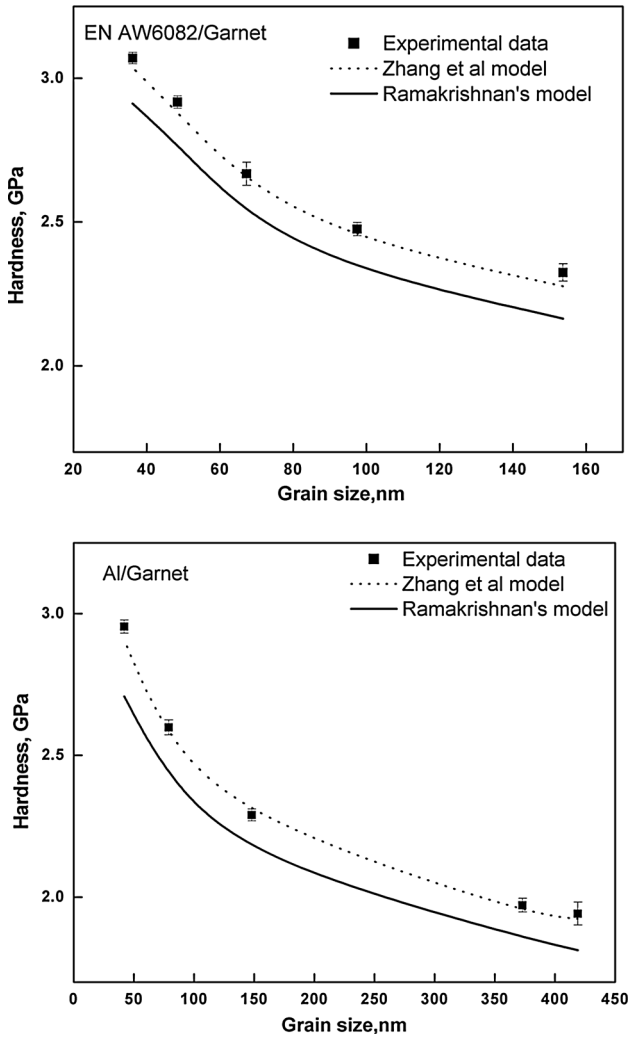

Fig. 14—Comparison of the model predictions *via* varying grain size with the experimental data for EN AW6082 and Al composite.

ening effect (f_{Orowan}), was also considered. Using Tabor relation,[45] hardness is assumed to correspond to the yield stress multiplied by a factor of three. Figure 14 shows the hardness predicted by the Zhang model, *i.e.*, Eq. [2], and Ramakrishna model in a garnet particulate-reinforced Al and EN AW6082 Al-alloy composite. The validity of the equation was checked against available experimental data and a reasonable agreement was observed with the values predicted by the model proposed by Zhang *et al.*, as shown in Figure 14. The accuracy of the estimation of hardness using model was well within an order of magnitude. This indicates that the calculations based on the strengthening mechanisms involving combined effect of load bearing, dislocation strengthening and Orowan strengthening can be used to accurately model the hardness of the present ball-milled particulate-reinforced composites.

F. *Nanohardness Measurement*

The hardness measurements were also performed using Nanoindentation tests on the milled powders.

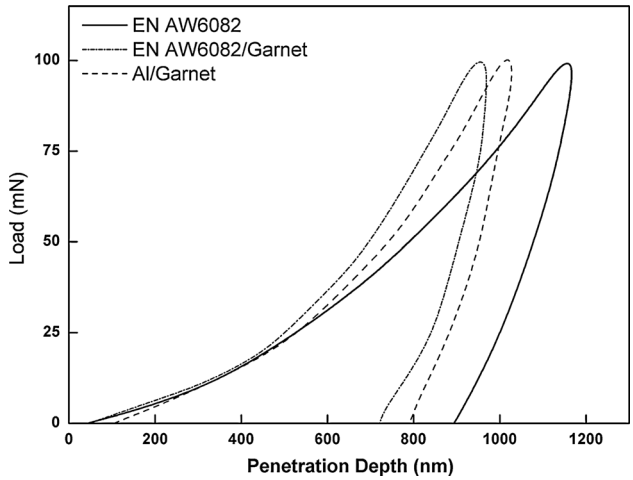

Fig. 15—Load *vs* penetration depth curves of unreinforced EN AW6082 and composite powders milled for 50 h.

Table VI. Elastic Modulus and Hardness of the Unreinforced Alloy and Composite Constituents MM for 50 h Measured by Nanoindentation

System	E (GPa)	H (GPa)
EN AW6082	104 ± 12	3.02 ± 0.4
EN AW6082/Garnet	148 ± 7	4.24 ± 0.07
Al/Garnet	127 ± 9	3.63 ± 0.1

Indentations were made at 10 different locations on the sample surface to provide a good statistical sampling. The hardness (H) was calculated from the maximum load (F_m) and the maximum penetration depth (h_m^2) by the formula.[21]

$$H = 0.03784 \cdot F_m / h_m^2. \quad [3]$$

The typical load–displacement curves for 50 hours milled unreinforced alloy and composite powders are shown in Figure 15. The curves are for the indentations made to peak load of 100 mN at room temperature and exhibit a typical elastic behavior. The differences in hardness of the milled powders are apparent from the large differences in peak depth. The elastic modulus and hardness, estimated from this curve, are given in Table VI. All the hardness and the elastic modulus values obtained are higher than that for pure aluminum, which has a hardness value of 0.7 GPa[51] and elastic modulus of 76 GPa.[52] Hence, parameters such as high-energy ball milling, addition of reinforcement and alloying elements has considerably increased the hardness values almost 1.57, 2.8, and 2.18 times for unreinforced and reinforced alloy and Al/garnet composite, respectively, compared to pure aluminum. Orowan strengthening, grain size and substructure strengthening, quench hardening resulting from the dislocations generated to accommodate the differential thermal contraction between the reinforcing particles and matrix, and

work hardening due to the strain misfit between the elastic reinforcing particles and the particle matrix[3] are the possible strengthening mechanisms which may operate simultaneously leading to increased hardness and elastic modulus. Difference in microhardness and nanohardness of milled powders could be due to indentation size effect (ISE).[53] Nanoindendation results show that the addition of garnet in EN AW6082 matrix increased the hardness and elastic modulus from 3.02 and 104 GPa to 4.24 and 148 GPa, respectively, after 50 hours of milling. With increase in milling time, the reinforcement particle size decreases, which have a positive effect on the mechanical properties of the composite powders.

IV. CONCLUSIONS

The influence of high-energy ball milling time on the morphological and structural features, lattice strain, crystallite size and mechanical properties of unreinforced and garnet reinforced EN AW6082 alloy and garnet reinforced pure Al powders has been investigated. The results of the above investigation have led to the following conclusions:

1. High-energy milling method, used for the preparation of composite powders with hard particle reinforcement resulted in refined microstructure and randomly oriented interfacial grain boundaries.
2. XRD evaluation did not indicate any phase transformation during milling of unreinforced EN AW6082, EN AW6082/Garnet, and Al/Garnet composite blends. However, α-Al peaks evidenced a shift in their original position. Intense effect was observed in unreinforced EN AW6082 alloy due to formation of supersaturated solid solution, contrary to other composite mixture where the peak shift is minimal due to presence of hard dispersoids.
3. The crystallite size of the aluminum alloy in the composite powder was smaller than that of the unreinforced alloy at the same milling time and the size reached to 36 nm for EN AW6082/Garnet after 50 hours milling.
4. Among the different composites investigated, EN AW6082/Garnet was found to be most effective in microstructural refinement and improved mechanical properties. The variation of hardness values with grain size follows the empirical Hall–Petch relationship.
5. Strengthening model prediction involving Orowan effect was found to be in agreement with the experimental data for both Al and Al-alloy composites synthesized by high-energy milling.

ACKNOWLEDGMENTS

The authors would like to thank Dr. A. Rajkumar, CSIR-NML Madras Centre, for providing the garnet powder and wish to express their gratitude to Dr. Ansu J. Kailath and Dr. Suman Kumari Mishra, CSIR-NML, Jamshedpur, for their valuable technical assistance.

REFERENCES

1. K.K. Chawla: *Composite Materials Science and Engineering*, 2nd ed., Springer, New York, 1997.
2. T.W. Clyne and P.J. Withers: *An Introduction to Metal Matrix Composites*, Cambridge University Press, Cambridge, 1993.
3. D.B. Miracle: *Compos. Sci. Technol.*, 2005, vol. 65, pp. 2526–40.
4. A. Heinz, A. Haszler, C. Keidel, S. Moldenhauer, R. Benedictus, and W.S. Miller: *Mater. Sci. Eng. A*, 2000, vol. 280, pp. 102–07.
5. D.J. Lloyd: *Mater. Rev.*, 1994, vol. 39, pp. 1–23.
6. J.M. Torralba, C.E. Da Costa, and F. Velasco: *J. Mater. Process. Technol.*, 2003, vol. 133, pp. 203–06.
7. J.J. Sobczak and L. Drenchev: *J. Mater. Sci. Technol.*, 2013, vol. 29, pp. 297–316.
8. L. Lu, M.O. Lai, and C.W. Ng: *Mater. Sci. Eng. A*, 1998, vol. 252, pp. 203–11.
9. S.A. Khadem, S. Nategh, and H. Yoozbashizadeh: *J. Alloys Compd.*, 2011, vol. 509, pp. 2221–26.
10. B. Prabhu, C. Suryanarayana, L. An, and R. Vaidyanathan: *Mater. Sci. Eng. A*, 2006, vol. 425, pp. 192–200.
11. M. Khakbiz and F. Akhlaghi: *J. Alloys Compd.*, 2009, vol. 479, pp. 334–41.
12. L.E.G. Cambronero, E. Sánchez, J.M. Ruiz-Roman, and J.M. Ruiz-Prieto: *J. Mater. Process. Technol.*, 2003, vols. 143–144, pp. 378–83.
13. A.K. Chaubey, S. Scudino, N.K. Mukhopadhyay, M. Samadi Khoshkhoo, B.K. Mishra, and J. Eckert: *J. Alloys Compd.*, 2012, vol. 536, pp. S134–S137.
14. M.H. Lee, J.H. Kim, J.S. Park, W.T. Kim, and D.H. Kim: *Mater. Sci. Forum*, 2005, vol. 475, pp. 3427–30.
15. F. Ali, S. Scudino, G. Liu, V.C. Srivastava, N.K. Mukhopadhyay, M. Samadi Khoshkhoo, K.G. Prashanth, V. Uhlenwinkel, M. Calin, and J. Eckert: *J. Alloys Compd.*, 2012, vol. 536, pp. S130–S133.
16. R. Perez-Bustamante, I. Estrada-Guel, W. Antunez-Flores, M. Miki-Yoshida, P.J. Ferreira, and R. Martinez-Sanchez: *J. Alloys Compd.*, 2008, vol. 450, pp. 323–26.
17. E. Rodrigues de Araujo, S.J. Ferreira Alves, F.A. Filho, S.L. Urtiga Filho, and O. Olimpio de Araujo Filho: *Eighth International Latin American Conference on Powder Technology*, Costao do Santinho, Florianopolis, SC, Brazil, 2011, pp. 325–30.
18. K.H.W. Seah, M. Krishna, V.T. Vijayalakshmi, and J. Uchil: *Corros. Sci.*, 2002, vol. 44, pp. 917–25.
19. S.C. Sharma: *Wear*, 2001, vol. 249, pp. 1036–45.
20. G.K. Williamson and W.H. Hall: *Acta Metall.*, 1953, vol. 1, pp. 22–31.
21. W.C. Oliver and G.M. Pharr: *J. Mater. Res.*, 2004, vol. 19, pp. 3–20.
22. R. Deaquino-Lara, I. Estrada-Guel, G. Hinojosa-Ruiz, R. Flores-Campos, J.M. Herrera-Ramirez, and R. Martinez-Sanchez: *J. Alloys Compd.*, 2011, vol. 509S, pp. S284–S289.
23. S. Sivasankaran, K. Sivaprasad, R. Narayanasamy, and V. Kumar Iyer: *J. Alloys Compd.*, 2010, vol. 491, pp. 712–21.
24. C. Suryanarayana: *Prog. Mater. Sci.*, 2001, vol. 46, pp. 1–184.
25. J.R. Ares and F. Cuevas: *Acta Mater.*, 2005, vol. 53, pp. 2157–67.
26. M. Delshad Chermahinia, S. Sharafia, H. Shokrollahi, M. Zandrahimia, and A. Shafyei: *J. Alloys Compd.*, 2009, vol. 484, pp. 54–58.
27. S.S. Razavi Tousi, R. Yazdani Rad, E. Salahi, I. Mosbasherpour, and M. Razavi: *Powder Technol.*, 2009, vol. 192, pp. 346–51.
28. N. Zhao, P. Nash, and X. Yang: *J. Mater. Process. Technol.*, 2005, vol. 170, pp. 586–92.
29. L. Wang and F.S. Li: *J. Magn. Magn. Mater.*, 2001, vol. 223, pp. 233–37.
30. B. Lonnberg: *J. Mater. Sci.*, 1994, vol. 29, pp. 3224–30.
31. H.J. Fecht: *Nanostruct. Mater.*, 1995, vol. 6, pp. 33–42.
32. W. Qin, Z.H. Chen, P.Y. Huang, and Y.H. Zhuang: *J. Alloys Compd.*, 1999, vol. 292, pp. 230–32.

33. J.B. Fogognolo, F. Velasco, M.H. Robert, and J.M. Torralba: *Mater. Sci. Eng. A*, 2003, vol. 342, pp. 131–43.
34. Z. Razavi Hesabi, A. Simchi, and S.M. Seyed Reihani: *Mater. Sci. Eng. A*, 2006, vol. 428, pp. 159–68.
35. A. Santos-Beltrán, V. Gallegos-Orozco, and I. Estrada-Guel: *J. Alloys Compd.*, 2006, vol. 435, pp. 514–17.
36. K.D. Woo and H.W. Huo: *Met. Mater. Int.*, 2006, vol. 12, pp. 45–50.
37. J.L. Hernandez, J.J. Cruz, C. Gomez, Y.O. Coreno, and R. Martinez-Sanchez: *Mater. Trans.*, 2010, vol. 51, pp. 1120–26.
38. M. Azabou, M. Khitouni, and A. Kolsi: *Mater. Charact.*, 2009, vol. 60, pp. 499–505.
39. R. Maiti and M. Chakraborty: *J. Alloys Compd.*, 2008, vol. 458, pp. 450–56.
40. J. Safari, G.H. Akbari, A. Shahbazkhan, and M. Delshad Chermahini: *J. Alloys Compd.*, 2011, vol. 509, pp. 9419–24.
41. M.F. Ashby: *Philos. Mag.*, 1970, vol. 21, pp. 399–424.
42. L.M. Brown and R.K. Ham: *Strengthening Methods in Crystals*, Elsevier, Amsterdam, 1971, pp. 9–135.
43. E.O. Hall: *Proc. Phys. Soc. (London)*, 1951, vol. B64, pp. 747–53.
44. N.J. Petch: *J. Iron Steel Inst.*, 1953, vol. 174, pp. 25–28.
45. D. Tabor: *The Hardness of Metals*, Oxford University Press, Oxford, 1951.
46. H. Abdoli, M. Ghanbari, and S. Baghshahi: *Mater. Sci. Eng. A*, 2011, vol. 528, pp. 6702–07.
47. Y.S. Sato, M. Urata, H. Kokawa, and K. Ikeda: *Mater. Sci. Eng. A*, 2003, vol. 354, pp. 298–305.
48. Z. Zhang and D.L. Chen: *Scripta Mater.*, 2006, vol. 54, pp. 1321–26.
49. Z. Zhang and D.L. Chen: *Sci. Technol. Adv. Mater.*, 2007, vol. 8, pp. 5–10.
50. N. Ramakrishnan: *Acta Mater.*, 1996, vol. 44, pp. 69–77.
51. L.F. Mondolfo: *Aluminium Alloys: Structure and Properties*, Butterworth, London, 1976.
52. S. Nayak, L. Riester, and N.B. Dahotre: *J. Mater. Res.*, 2004, vol. 19, pp. 202–07.
53. N.K. Mukhopadhyay and P. Paufler: *Intern. Mater. Rev.*, 2006, vol. 51, pp. 209–45.